SPECTA Journal of Technology Vol 10, No 2 August, 2026 pg: 199 – 224
DOI: 10.35718/specta.v10i2.8481915

SPECTA Journal of Technology
E-ISSN : 2622-9099
P-ISSN : 2549-2713
Homepage jurnal: https://journal.itk.ac.id/index.php/sjt

Identification of Mass Movement Susceptibility Zones Using Geotechnical Investigation and the Weight of Evidence (WoE) Method in Sambutan District, Samarinda, East Kalimantan

Diftania Avanda Ayu Shinta[1], Muhammad Rizqy Septyandy[2*], Muhammad Amin Syam[3], Aji Muhammad Rifqi Abdillah[4], Pridawanti Ayuningtyas[5], Panggea Ghiyats Sabrian[6]

[12*3456]Geological Engineering Program Study, Faculty of Engineering, Universitas Mulawarman, Samarinda, Indonesia.

Corresponding email: *rizqyseptyandy@ft.unmul.ac.id*

Received: 17/January/2026 Revised: 01/August/2026
Accepted: 21/August/2026 Published: 31/August/2026

To cite this article:
Shinta, D. A. A., Septyandy, M. R., Syam, M. A., Abdillah, A. M. R., Ayuningtyas, P & Sabrian, P. G. (2026). Identification of Landslide-Prone Areas in Sambutan District, Samarinda, East Kalimantan. *SPECTA Journal of Technology,* 10(2), 199-224. 10.35718/specta.v10i2.8481915

Abstract

Sambutan District, Samarinda City, occupies undulating to hilly terrain underlain by weakly consolidated Tertiary sediments, and has recorded 33 mass movement events over the last five years. Existing susceptibility studies in the region rely almost entirely on terrain and remote sensing variables, so the mechanical behaviour of the slope-forming materials is rarely represented. This study combines field and laboratory geotechnical investigation with a Weight of Evidence (WoE) spatial model to map mass movement susceptibility at a scale usable for local spatial planning. Fifteen observation stations were selected by purposive sampling across the recorded inventory and the mapped landform units. Each station was investigated using the Cone Penetration Test (CPT), soil physical property tests, and the Direct Shear Test, and slope stability was analysed with the Morgenstern-Price method using the surveyed slope geometry. Thirteen conditioning factors were weighted using WoE and screened by their individual Area Under the Curve (AUC) values. Slope angle and slope aspect (AUC 0.898 each) and elevation (0.7475) were retained as dominant controls, and the final model reached an AUC of 0.863. The resulting map classifies 62.05 km² (54.72%) of the area as low susceptibility, 9.98 km² (8.80%) as moderate, and 41.37 km² (36.48%) as high. Twelve of the fifteen stations are clay or silty clay of moderate to high plasticity, with plasticity index between 4.07 and 26.68% and cohesion below 0.6 kPa at every station. Stability is governed by the ratio of internal friction angle to slope angle rather than by cohesion: $\tan \varphi / \tan \beta$ correlates with the factor of safety at $r = 0.773$ ($p = 0.001$) while cohesion does not ($r = 0.071$, $p = 0.803$). Six stations return a factor of safety below 1.07, and every station on ground steeper than 40° is unstable, the unstable group averaging 45.5° against 33.3° for the stable one ($p = 0.016$). On this basis the paper proposes cut slope limitation, mandatory site-specific geotechnical investigation, and slope drainage requirements for the high susceptibility zone, which can be adopted directly into the RTRW and RDTR of Samarinda City.

Keywords: mass movement susceptibility, Weight of Evidence, cone penetration test, direct shear test, spatial planning, Samarinda.

1. Introduction

Indonesia sits on the Pacific Ring of Fire and in the humid tropics, a combination that produces frequent slope failures during periods of prolonged rainfall. Samarinda City is not a seismically active area, but it is underlain by weakly consolidated Tertiary sediments and receives more than 2,000 mm of rain per year, so mass movement here is driven mainly by rainfall, weathering, and human modification of slopes.

Sambutan District has changed rapidly over the past decade. Residential blocks, new access roads, and land clearing have replaced vegetated hillslopes, which reduces root reinforcement, increases surface runoff, and adds load to slope crests. According to the Badan Penanggulangan Bencana Daerah (BPBD) of Samarinda City, 33 mass movement events were recorded in the district during the last five years. These events damaged houses, agricultural land, and road infrastructure, and one fatality was reported at the end of 2022. Losses of this kind are concentrated in areas that the current Rencana Tata Ruang Wilayah (RTRW) still designates for residential expansion, which means that the hazard information available to the planning authority is not detailed enough to guide permits at the neighbourhood scale.

Mass movement is the gravity-driven downslope displacement of rock, debris, or soil, and includes falls, topples, slides, lateral spreads, and flows (Cruden & Varnes, 1996). Its distribution is governed by the interaction of topography, lithology, hydrology, land cover, and the engineering properties of the slope-forming material, so a susceptibility assessment has to represent several of these controls at once.

Susceptibility mapping has been carried out with bivariate statistical models, logistic regression, and machine learning. Wubalem and Meten (2020) applied information value and logistic regression in northwestern Ethiopia; Saha et al. (2020) compared the analytical hierarchy process, frequency ratio, logistic regression, and their ensembles; Ling et al. (2022) used a random forest algorithm for geohazard susceptibility in Tianshui, China; and Liao et al. (2022) tested hybrid machine learning at several grid resolutions in Wushan and Wuxi counties. In Indonesia, Kusmajaya et al. (2022) mapped landslide hazard in Sukabumi Regency using WoE, logistic regression, and a combined WoE-LR model. Karunarathna et al. (2024) took a different route and identified potential failure zones from LiDAR-derived slope shading in Kegalle, Sri Lanka. A summary of these studies is given in Table 1.

Two limitations follow from that body of work. First, the input variables are almost always derived from terrain models, satellite imagery, and thematic maps, while subsurface parameters such as cone resistance, Atterberg limits, cohesion, and internal friction angle are seldom measured at all. The resulting maps therefore describe where failures have occurred without describing why the material fails. Second, no published susceptibility assessment covers Sambutan District at a resolution that a Rencana Detail Tata Ruang (RDTR) could use, even though the district is the main direction of residential growth in eastern Samarinda. This study addresses both points by measuring the geotechnical properties of the slope-forming materials at fifteen stations and using those measurements to interpret and cross-check a WoE susceptibility model.

The Weight of Evidence method was selected for three reasons. It is a data-driven bivariate model, so the weights come from the observed spatial association between the inventory and each factor class rather than from expert judgement, which removes the subjectivity of scoring methods such as the analytical hierarchy process. The positive and negative weights and the contrast value are directly interpretable, so a planner can see which factor class contributes to the hazard and by how much. And the method performs reliably with inventories of modest size, which matters here because the district has 33 recorded events (Bonham-Carter, 1994; Regmi et al., 2010; Pourghasemi et al., 2013). Kusmajaya et al. (2022) reported that WoE performed comparably to logistic regression in a West Java setting with similar data availability.

The objectives of this study are to determine the geotechnical characteristics of the slope-forming materials in Sambutan District, to identify the conditioning factors most strongly associated with recorded mass movements using WoE, to produce and validate a susceptibility map for the district, and to translate the result into recommendations that can be adopted in local spatial planning documents.

2. Study Literature

2.1 Previous Studies on Mass Movement Susceptibility

Table 1 summarises the studies most relevant to the present work, the variables they used, the validation they reported, and whether subsurface geotechnical data were included.

Table 1. Selected Previous Studies on Mass Movement Susceptibility Mapping

Study	Location	Method	Conditioning factors used	Validation	Geotechnical data included
Wubalem & Meten (2020)	Goncha Siso Eneses, Ethiopia	Information value, logistic regression	Slope, aspect, curvature, lithology, land use, distance to road/river	AUC 0.826 (IV), 0.884 (LR)	No
Saha et al. (2020)	Eastern Himalaya, India	AHP, frequency ratio, logistic regression, ensembles	12 terrain, hydrological, and land cover factors	ROC/AUC	No
Ling et al. (2022)	Tianshui, Gansu, China	Random forest	Terrain, geology, land cover, NDVI	ROC/AUC	No
Liao et al. (2022)	Wushan and Wuxi, China	Hybrid machine learning at several grid resolutions	Terrain, lithology, hydrology	ROC/AUC	No
Kusmajaya et al. (2022)	Sukabumi Regency, Indonesia	WoE, logistic regression, WoE-LR	Slope, lithology, soil, rainfall, land use	ROC/AUC	No
Karunarathna et al. (2024)	Kegalle, Sri Lanka	Geomorphological analysis of LiDAR slope shading	Terrain derivatives	Field verification	No
This study	Sambutan, Samarinda, Indonesia	WoE with geotechnical characterisation	13 factors plus CPT, Atterberg limits, direct shear, factor of safety	AUC 0.887	Yes

The pattern in Table 1 is consistent. Terrain and land cover variables dominate, validation is reported as an AUC value, and the mechanical properties of the failing material are left out. Van Westen et al. (2003) noted the same problem and argued that indirect susceptibility maps become far more usable once they are tied to material behaviour. The present study follows that recommendation.

2.2 Regional Geological Setting

The regional geology is taken from the Geological Map of the Samarinda Sheet at 1:250,000 (Supriatna et al., 1995). Four units crop out in the study area: the Pulaubalang Formation (Tmpb), the Balikpapan Formation (Tmbp), the Kampung Baru Formation (Tpkb), and Quaternary Alluvium (Qa), shown in Figure 1.

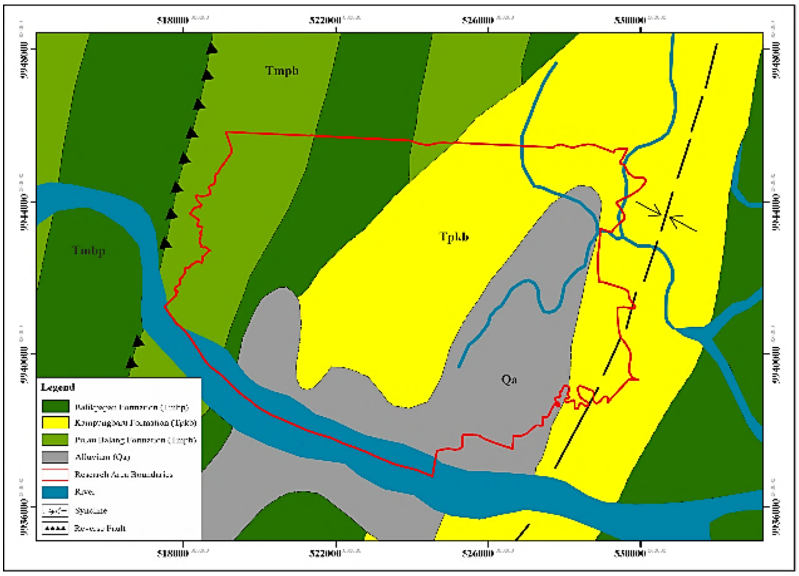

Figure 1. Regional Geology of the Study Area (Supriatna et al., 1995)

The Pulaubalang Formation consists of greywacke, quartz sandstone, limestone, claystone, and coal. The Balikpapan Formation is made up of alternating sandstone and claystone with interbeds of shale, siltstone, limestone, and coal. The Kampung Baru Formation is dominated by quartz sandstone interbedded with claystone, shale, and lignite, generally deeply weathered and easily disaggregated. The Quaternary Alluvium consists of unconsolidated gravel, sand, silt, and clay in lowland and fluvial settings (Supriatna et al., 1995). Because the whole succession belongs to the Kutai Basin, the lithologies are texturally similar and poorly cemented, which is consistent with the narrow range of specific gravity measured in this study.

Figure 1 is not one of the thirteen conditioning factors in the WoE model. Its function in this paper is to explain the origin of the soil type layer that is used as a factor: the soils tested at the fifteen stations are residual and colluvial materials weathered from these four units, so the geological map provides the framework for interpreting why the soil classes behave differently.

2.3 Classification of Mass Movement

Cruden and Varnes (1996) classified mass movement into falls, topples, slides, spreads, and flows on the basis of the type of movement and the material involved. The classification is reproduced in Figure 2.

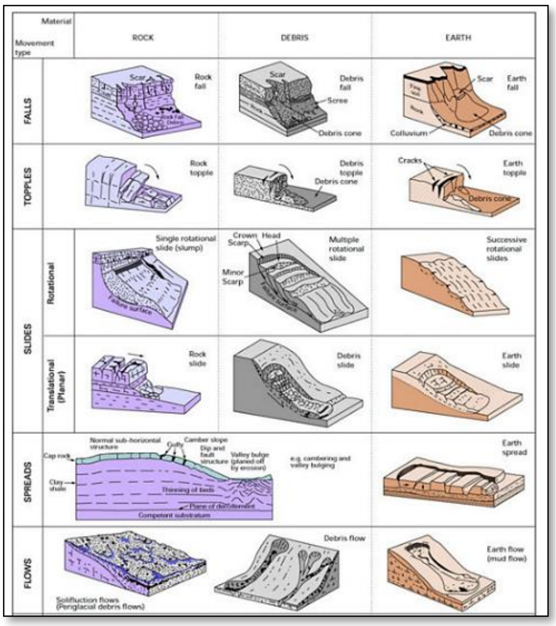

Figure 2. Types of Mass Movement (Cruden & Varnes, 1996)

Figure 2 is used in two ways. It provides the criteria applied in Section 4.1 to classify each of the fifteen field stations, and it defines the scope of the model. Because the inventory contains slides, falls, and flows rather than a single mechanism, the WoE model produces a general mass movement susceptibility map, not a map for one failure type. Priyono (2015) made the same distinction between landslide classification and the classification of landslide-prone ground.

2.4 Conditioning Factors

Slope gradient is the dominant topographic control, since it determines the ratio of the driving component of gravity to the resisting shear strength (Liao et al., 2022). Elevation does not cause failure directly, but it discriminates between terrain units with different relief energy and different weathering depths (Niu et al., 2018). Soil type controls the physical response of the surface material: poorly consolidated soils lose strength and disaggregate when wetted, which raises failure likelihood (Wubalem & Meten, 2020). Lineaments mark surface expressions of structures along which rock is more fractured and more permeable, and are mapped from adjacent linear patterns visible on imagery and shaded relief. NDVI and NDBI describe vegetation cover and built-up density, which affect root reinforcement, infiltration, and imposed load (Akbar et al., 2019). Distance to rivers represents toe erosion and the elevated pore pressure of the near-channel zone, and distance to roads represents cut slopes and undercutting.

2.5 Soil Physical Properties

Physical properties are those measurable without altering the chemical composition of the soil, and they govern bearing capacity and the stability of structures founded on the soil (Murthy, 2006). In this study the tests followed Indonesian National Standards: water content (SNI 1965:2008), specific gravity (SNI 1964:2008), unit weight (SNI 8460:2017), liquid limit (SNI 1967:2008), plastic limit (SNI 1966:2008), and shrinkage limit (SNI 3422:2008).

Water content (w) is the ratio of the mass of water to the mass of dry soil particles, expressed as a percentage (Das, 2010):

$$w = \frac{w_2 - w_3}{w_3 - w_1} \times 100 \quad (1)$$

where:

w = water content (%)

w_1 = weight of empty dish (g)

w_2 = mass of dish and wet soil (g)

w_3 = mass of dish and oven-dried soil (g)

Specific gravity (Gs) is the ratio of the mass of soil particles to the mass of an equal volume of water at a stated temperature:

$$G_s = \frac{w_t}{w_t + (w_4 - w_3)} \times A \quad (2)$$

where:

w_t = mass of soil

w_4 = mass of pycnometer and water at T °C

w_3 = mass of pycnometer, water, and soil

A = specific gravity of water at T °C

The consistency limits describe the water contents at which a fine-grained soil changes state, and depend on the attraction between clay mineral particles (Das, 2010). The positions of the limits are shown in Figure 3.

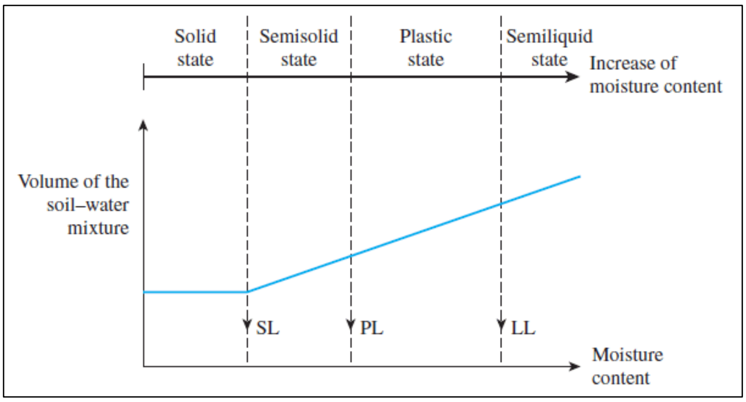

Figure 3. Atterberg Limit (after Das, 2010)

The liquid limit (LL) is the water content at the boundary between the plastic and liquid states, and can be classified using Whitlow (1995), as given in Table 2.

Table 2. Liquid Limit Classification (Whitlow, 1995)

Liquid Limit	Category
<35%	Low Plasticity
35% - 50%	Medium Plasticity
50% - 70%	High Plasticity
70% - 90%	Very High Plasticity
>90%	Extremely high Plasticity

The plastic limit (PL) is the water content at which a soil thread crumbles when rolled to 3.2 mm diameter. The plasticity index (PI = LL − PL) increases with clay content and with the capacity of the soil to hold water while remaining plastic (Hardiyatmo, 1995). Table 3 relates PI to soil type.

Table 3. Relationship Plasticity Index and Soil Type (Hardiyatmo, 1995)

Soil Type	Cohesion	Plasticity	PI
Sand	Non-cohesive	Non-plastic	0
Silt	Slightly cohesive	Low	< 7
Silty Clay	Cohesive	Moderate	7-17
Pure Clay	Cohesive	High	> 17

The shrinkage limit (SL) is the water content below which further drying produces no volume change. It is used to assess expansion potential (Table 4), which matters on slopes because shrink-swell cycles open desiccation cracks that admit rainwater directly to the potential slip surface.

Table 4. Classification of Expansion Potential (Altmever, 1955)

Shrinkage Limit (%)	Degree of Expansion
<10	Critical
10 - 12	Moderate
>12	Non-Critical

2.6 Cone Penetration Test

The Cone Penetration Test (CPT) determines the mechanical properties of the subsurface without drilling. It records cone resistance (q_c or, corrected, q_t), sleeve friction (f_s), pore pressure (u), and the friction ratio $R_f = f_s/q_c$, from which the soil behaviour type index I_c is derived and the soil profile is classified (Robertson et al., 1986; Robertson, 1990; Lunne et al., 2014). Testing stops when cone resistance reaches the capacity of the equipment or when the target depth is reached (Gofar & Ismail, 2022).

2.7 Shear Strength and Slope Stability

Shear strength is the maximum shear stress a soil can sustain before failure. The direct shear test provides cohesion (c) and the internal friction angle (φ) for use in the Mohr-Coulomb criterion, in which shear strength is a function of effective normal stress, φ, and c (Tania & Wulandari, 2020).

Slope stability is expressed as the factor of safety (FS), the ratio of resisting to driving forces on the potential slip surface (Das, 2010). FS was computed with the Morgenstern-Price method, a limit equilibrium procedure that satisfies both force and moment equilibrium for every slice and assumes a functional relationship between the interslice shear force X and the interslice normal force E (Morgenstern & Price, 1965; Allan Takwin et al., 2017). The classification used here follows Bowles (1989) in Zakaria et al. (2018), given in Table 5.

Table 5. Factor of Safety Criteria (Bowles, 1989 in Zakaria et al., 2018)

Factor of safety (FS)	Slope Conditions	Interpretation
FS < 1.07	Failure occurs commonly	Unstable
1.07 < FS < 1.25	Failure has occurred	Critical
FS > 1.25	Failure is rare	Safe

2.7 Weight of Evidence and Model Validation

Weight of Evidence is a log-linear Bayesian model that quantifies the spatial association between an inventory of events and each class of a conditioning factor, under the assumption that the factors are conditionally independent given the inventory (Bonham-Carter, 1994). It uses a prior probability, derived from the inventory alone, which is then updated with the evidence contributed by each factor class to give a posterior probability. The formulation is set out in Section 3.6.

Model performance is measured by the Area Under the Curve (AUC) of the Receiver Operating Characteristic curve. Higher AUC values indicate better discrimination between areas that did and did not fail. The index used here follows Yesilnacar and Topal (2005) in Pourghasemi et al. (2013), given in Table 6.

Table 6. AUC Index Values (Yesilnacar & Topal, 2005, in Pourghasemi et al., 2013)

AUC Value	Label
> 0.9	Excellent
0.8 – 0.9	Good
0.7 – 0.8	Fair
0.6 – 0.7	Poor
< 0.6	Fail

3. Method

3.1 Study Area and General Approach

The study covers Sambutan District, Samarinda City, an area of approximately 113.4 km² of undulating to hilly terrain in the eastern part of the city. The work combines a field and laboratory geotechnical investigation with a GIS-based bivariate statistical analysis. The full sequence of input, process, and output is given in Figure 5 and described below.

3.2 Data and Data Sources

Primary data were collected in the field; secondary data were obtained from national agencies and satellite imagery. Table 7 lists every dataset, its source and resolution, and the conditioning factor derived from it.

Table 7. Data Sources and Derived Conditioning Factors

No.	Data	Source	Scale / Resolution	Derived Factor or Use
1	DEMNAS	Badan Informasi Geospasial	8.3 m (0.27 arc-second)	Elevation, slope angle, slope aspect, plan curvature, profile curvature
2	Rainfall (annual, 10 years)	BMKG Samarinda station	Point data, interpolated	Rainfall

No.	Data	Source	Scale / Resolution	Derived Factor or Use
3	Landsat 8 OLI imagery	USGS Earth Explorer	30 m	NDVI, NDBI
4	Land cover map	Ministry of Environment and Forestry / on-screen digitising	1:50,000	Land cover
5	Soil type map	Balai Besar Litbang Sumberdaya Lahan Pertanian	1:50,000	Soil type
6	River and road network	Rupabumi Indonesia (RBI)	1:25,000	Distance to rivers, distance to roads
7	Lineament interpretation	DEMNAS shaded relief, multi-azimuth	8.3 m	Distance to lineaments
8	Geological map, Samarinda Sheet	Supriatna et al. (1995)	1:250,000	Geological framework (not a model input)
9	Mass movement inventory (33 events)	BPBD Samarinda + field verification	Point data	Dependent variable, model training and validation
10	CPT, soil physical properties, direct shear	Field and laboratory work, 15 stations	Point data	Material characterisation and factor of safety

All spatial layers were projected to WGS 1984 UTM Zone 50S and resampled to a common 10 m cell size before the WoE computation, so that pixel counts are comparable across factors. Analysis was carried out in ArcGIS; slope stability was computed in Slide; CPT records were processed in CLiq.

3.3 Sampling Design

The fifteen observation stations were selected by purposive sampling rather than by a regular grid. A grid design was rejected because a bivariate susceptibility model requires material data from the places where failure has actually occurred or is most likely, and a uniform grid would have spent most of its stations on the flat alluvial plain, where the mass movement inventory is empty. Purposive selection also reflects the practical constraints of hand auger sampling and CPT mobilisation on steep, partly forested ground.

Three criteria were applied in choosing the stations. Each station had to coincide with, or lie immediately adjacent to, a mass movement recorded in the BPBD inventory or identified during reconnaissance, so that the material tested is the material that failed. The set as a whole had to cover the landform units mapped in the study area, following the terrain classification principles of Zuidam (1985), and the range of slope gradients present in the district. The stations also had to be distributed across the three preliminary susceptibility classes, so that low, moderate, and high susceptibility zones are each represented by tested material rather than only the high class.

Fifteen stations satisfy these criteria. The number follows from the geometry of the district: the inventory contains 33 events, which cluster into fifteen separate slope segments once events within the same segment and the same landform unit are grouped, and one station was placed in each segment. Sampling was therefore driven by the number of distinct failure settings, not by a predetermined figure. Every station was sampled with a manual hand auger to the depth of refusal, and the distribution of stations against the inventory is shown in Figure 4.

DOI: 10.35718/specta.v10i2.8481915

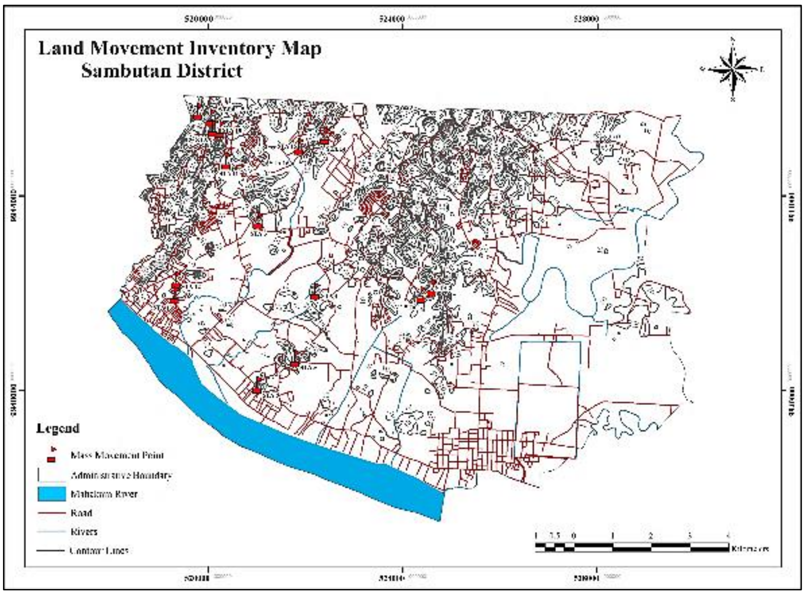

Figure 4. Mass Movement Inventory and Location of the Fifteen Observation Stations

The location, administrative unit, and surveyed slope angle of each station are given in Table 8. Coordinates were recorded in geographic form on the WGS 1984 datum and converted to WGS 1984 UTM Zone 50S for the spatial analysis.

Table 8. Location and Slope Geometry of the Fifteen Observation Stations (WGS 1984 UTM Zone 50S)

Station	Sub-District	Easting (m)	Northing (m)	Latitude	Longitude	Slope angle (°)
STA 1	Pulau Atas	524381.61	9941758.40	0°31’36.93”S	117°13’08.83”E	29
STA 2	Pulau Atas	524156.83	9941613.17	0°31’41.66”S	117°13’01.56”E	33
STA 3	Sambutan	520703.14	9943190.67	0°30’50.29”S	117°11’09.82”E	27
STA 4	Sambutan	521908.60	9941682.77	0°31’39.40”S	117°11’48.82”E	55
STA 5	Pulau Atas	521481.61	9940255.50	0°32’25.89”S	117°11’35.01”E	59
STA 6	Sungai Kapih	520686.90	9939699.11	0°32’44.01”S	117°11’09.30”E	39
STA 7	Sambutan	519294.96	9945520.69	0°29’34.40”S	117°10’24.26”E	25
STA 8	Sambutan	519703.09	9945365.72	0°29’39.45”S	117°10’37.46”E	37
STA 9	Sambutan	519737.36	9945137.14	0°29’46.89”S	117°10’38.57”E	31
STA 10	Sambutan	519894.03	9945119.67	0°29’47.46”S	117°10’43.64”E	34
STA 11	Sambutan	520035.10	9944445.21	0°30’09.43”S	117°10’48.21”E	26
STA 12	Sungai Kapih	518970.83	9941724.30	0°31’38.05”S	117°10’13.77”E	45
STA 13	Sungai Kapih	518930.77	9941602.28	0°31’42.02”S	117°10’12.48”E	36
STA 14	Sambutan	522121.79	9944972.82	0°29’52.24”S	117°11’55.72”E	40
STA 15	Sambutan	521565.20	9944758.74	0°29’59.22”S	117°11’37.71”E	47

The stations span slope angles from 25° to 59° and slope heights from 2.69 to 15.87 m, and lie in three clusters within a 5.5 by 5.8 km area, in Kelurahan Sambutan (eight stations), Kelurahan Pulau Atas (three), and Kelurahan Sungai Kapih (three). The clusters follow the dissected hills rather than the alluvial plain, which is the intended outcome of the sampling design. The slope-forming bedrock is sandstone at eight stations, interbedded sandstone and claystone at three, and claystone at one; bedding was measurable at six stations and the sequence is unbedded or massive at the rest.

The limitation of this design should be stated plainly. Because the stations were placed at or near known failures, the geotechnical dataset is deliberately biased towards unstable slopes and the proportion of stations returning a low factor of safety is not an estimate of the proportion of the district that is unstable. The geotechnical data explain the behaviour of the material in the susceptible zones; the areal proportions come from the spatial model.

3.4 Field and Laboratory Testing

Cone penetration testing was carried out in situ at four of the fifteen stations by a specialist contractor, with cone resistance, sleeve friction, and pore pressure logged continuously until refusal. The four stations were chosen to represent the range of profiles present rather than to cover every station, because CPT mobilisation on steep, partly forested ground is not practicable at every location. Disturbed and undisturbed samples were recovered by hand auger for laboratory testing at the Civil Engineering Laboratory, Faculty of Engineering, Universitas Mulawarman. Disturbed and undisturbed samples were recovered by hand auger at all fifteen stations. The laboratory programme, which took about fourteen days, comprised water content, specific gravity, unit weight, and the Atterberg limits, following the SNI standards listed in Section 2.5, and the direct shear test following SNI 2813:2008 to obtain c and φ. Slope height, length, width, and angle were measured at every station with a tape and compass for use in the stability analysis.

3.5 Slope Stability Analysis

The measured c, φ, and unit weight, together with the surveyed slope geometry, were entered into a two-dimensional limit equilibrium model for each station and solved by the Morgenstern-Price method to obtain the factor of safety. Results were classified with the criteria in Table 5.

3.6 Weight of Evidence formulation

For a conditioning factor class B and the presence of mass movement L, the positive weight W^+ measures the association between the presence of the class and the presence of failure, and the negative weight W^- measures the association between the absence of the class and the presence of failure:

$$W^+ = \ln\frac{P(B|L)}{P(B|\bar{L})} \quad (3)$$

$$W^- = \ln\frac{P(\bar{B}|L)}{P(\bar{B}|\bar{L})} \quad (4)$$

In pixel terms, with Npix1 the number of mass movement pixels inside the class, Npix2 the number of mass movement pixels outside the class, Npix3 the number of pixels inside the class without mass movement, and Npix4 the number of pixels outside the class without mass movement:

$$W^+ = \ln\frac{Npix1/(Npix1+Npix2)}{Npix3/(Npix3+Npix4)} \quad (5)$$

$$W^- = \ln\frac{Npix2/(Npix1+Npix2)}{Npix4/(Npix3+Npix4)} \quad (6)$$

The contrast C expresses the net spatial association of the class with mass movement, and is positive where the class favours failure and negative where it does not:

$$C = W^+ - W^- \quad (7)$$

The significance of the contrast was checked with the studentised contrast, C divided by its standard deviation, where $s^2(W^+) = 1/Npix1 + 1/Npix2$ and $s^2(W^-) = 1/Npix3 + 1/Npix4$:

$$C_{std} = \frac{C}{\sqrt{s^2(W^+)+s^2(W^-)}} \quad (8)$$

Classes with a studentised contrast below 1.96 were treated as not significantly associated with mass movement at the 95% level. The susceptibility index for every pixel is the sum of the weights of the classes that pixel falls into across the retained factors:

$$MMSI = \sum_{i=1}^{n} W_i \quad (9)$$

The index was then reclassified into three susceptibility levels using the thresholds of BNPB (2019): low (< 0.333), moderate (0.333–0.666), and high (> 0.666), after normalising the index to the 0–1 range.

SPECTA Journal of Technology Vol 10, No 2 August, 2026 pg: 199 – 224
DOI: 10.35718/specta.v10i2.8481915

3.7 Integration Of The Geotechnical Data with The Spatial Model

The fifteen stations were not interpolated into a continuous surface and were not entered as a WoE layer. Fifteen points spread over 113 km² of dissected terrain are too few and too unevenly distributed for interpolation to produce a defensible surface, and an interpolated layer would also violate the conditional independence assumption because it would partly duplicate the soil type and slope layers already in the model.

The geotechnical data are used in two other ways. They attribute the soil type layer: each station was assigned to a soil map unit, and the measured plasticity index, cohesion, and friction angle characterise that unit, so the WoE weights of the soil type classes can be read in terms of measured material behaviour rather than map labels. And they provide an independent physical check on the model output, since the station-scale factor of safety is compared with the susceptibility class assigned to the same location by the map, which tests whether the statistical zonation agrees with limit equilibrium analysis at points where both are available. This comparison is reported in Section 4.6.

3.8 Model Validation

The predictive performance of the model was evaluated with the ROC curve. The inventory was divided into a training subset used to compute the weights and a validation subset withheld from the computation, and the susceptibility index was compared against both subsets to obtain the success rate and prediction rate curves. The AUC was read from the resulting curve and interpreted with Table 6. The same procedure was applied to each of the thirteen factors individually, and factors with an individual AUC below 0.7 were excluded from the final overlay.

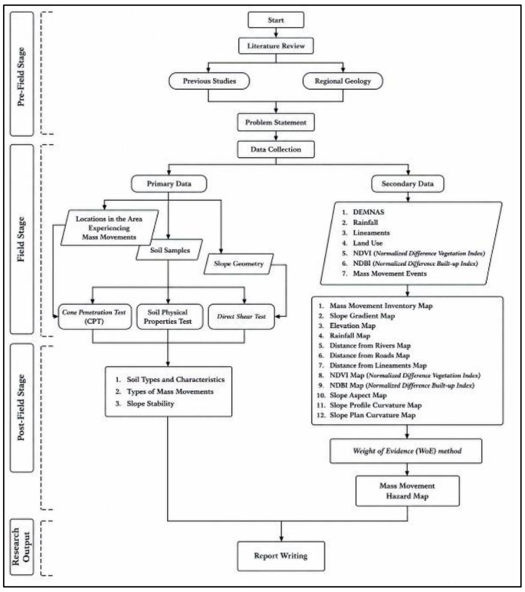

Figure 5. Research Flowchart Showing the Input, Process, and Output Stages

4. Result and Discussion

4.1 Types and Distribution of Mass Movement

Following the criteria of Cruden and Varnes (1996), four movement types were identified at the fifteen stations. Debris slides occur at STA 1, 2, 3, 6, 8, 9, 10, and 13; successive rotational slides at STA 5, 7, 14, and 15; rock and debris falls at STA 4 and STA 12; and an earth slide at STA 11. Slides therefore account for thirteen of the fifteen sites.

The distribution is not random. The debris slides are concentrated on the mid-slope segments of the Kampung Baru and Balikpapan Formations, where a residual mantle overlies weathered sandstone and the contact acts as a preferential slip surface during rainfall; sandstone or interbedded sandstone and claystone forms the slope at every one of these sites. Slope angle separates the groups. The two fall sites, STA 4 and STA 12, occupy the steepest measured faces at 55° and 45°, both on bedded sandstone dipping at 5° and 50° respectively, and at both the material detaches without a well-defined slip surface.

Three of the four rotational slides (STA 5, 14, 15) sit between 40° and 59°, whereas the debris slides occupy slopes of 27° to 41°. The single earth slide at STA 11 lies on the gentlest slope in the set, 26°, on claystone, and is the only site where the internal friction angle falls below 10°. Figure 6 shows the spatial pattern and Figure 7 shows stability with type and geometry.

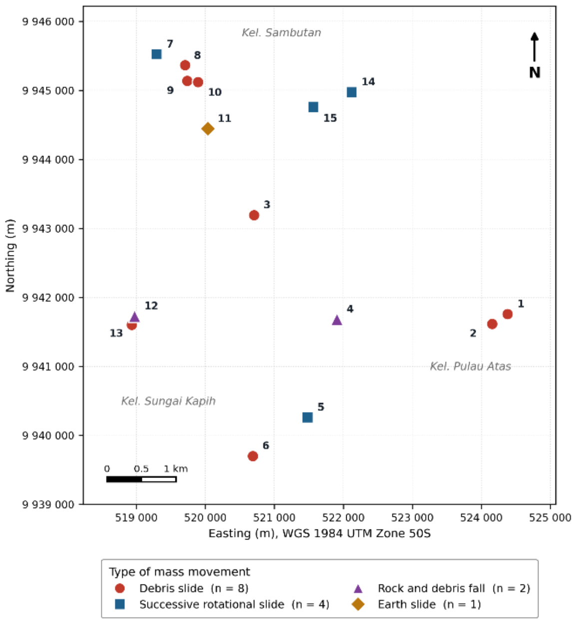

Figure 6. Distribution of Mass Movement Types at the Fifteen Observation Stations, Sambutan District (WGS 1984 UTM Zone 50S)

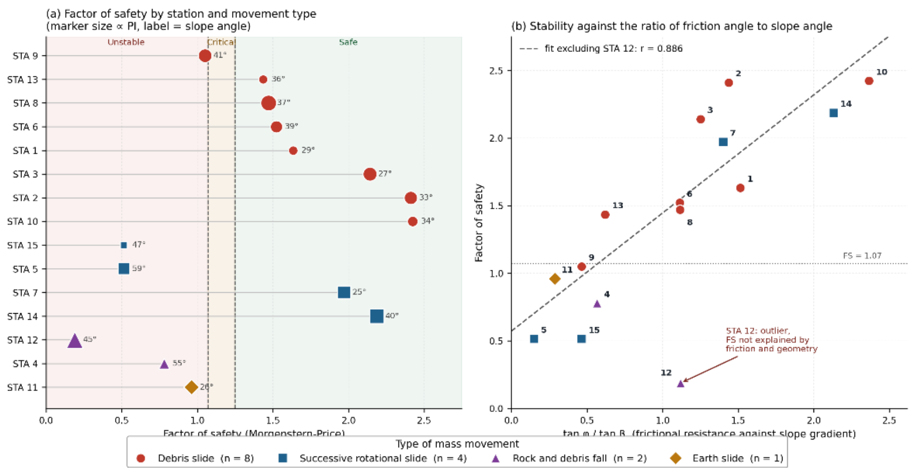

Figure 7. (a) Distribution of Factor of Safety by Station and Movement Type, **(b)** Stability Against the Ratio of Friction Angle to Slope Angle

4.2. Conditioning Factors

Thirteen factors were prepared as raster layers: elevation, slope angle, slope aspect, plan curvature, profile curvature, rainfall, soil type, land cover, NDVI, NDBI, distance to rivers, distance to roads, and distance to lineaments. They were chosen because they represent the topographic, hydrological, structural, land cover, and anthropogenic controls on slope stability discussed in Section 2.4, and because each could be derived consistently across the whole district from the sources in Table 7. The layers are shown in Figure 8.

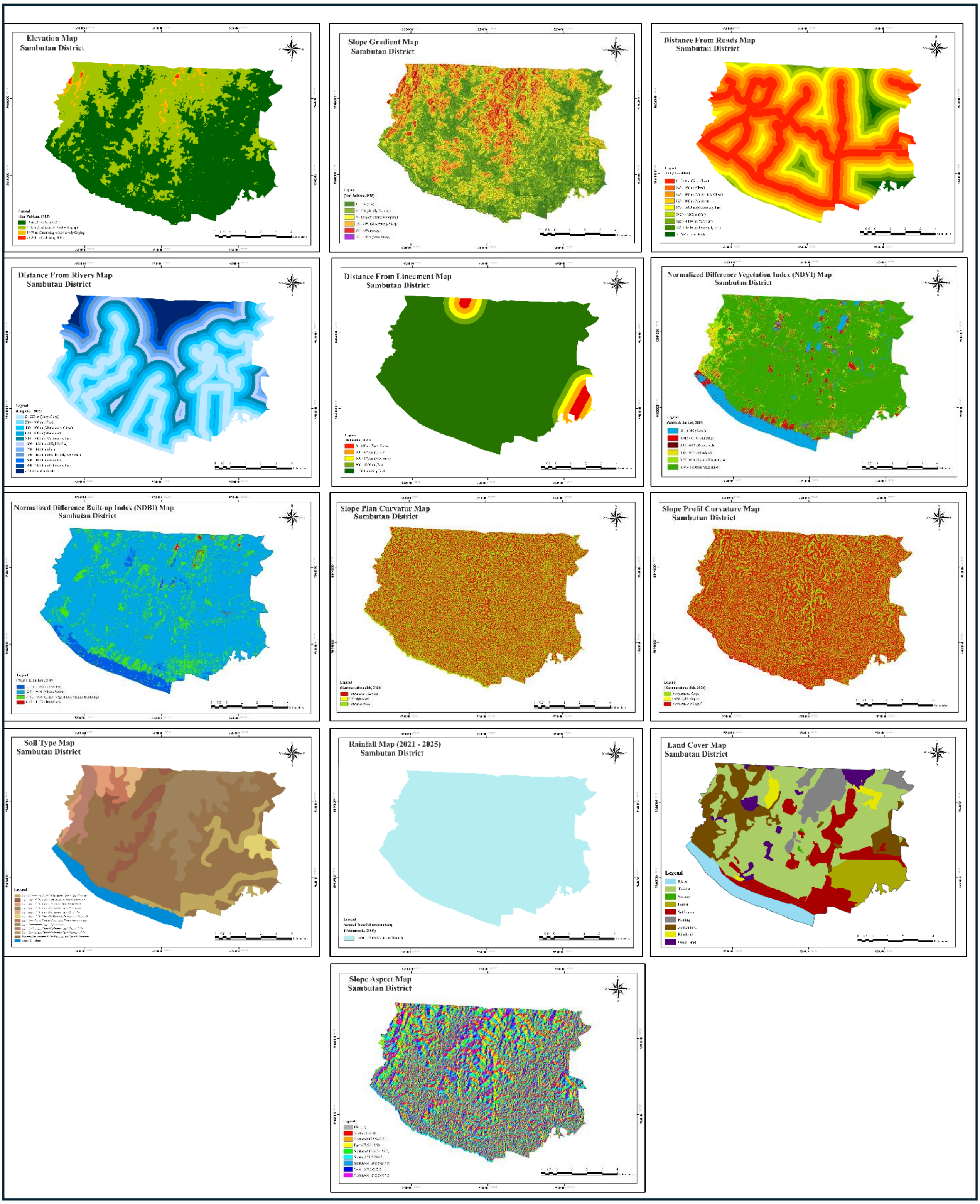

Figure 8. Conditioning Factors Used in the Analysis: (a) Elevation, (b) Slope Angle, (c) Slope Aspect, (d) Plan Curvature, (e) Profile Curvature, (f) Rainfall, (g) Soil Type, (h) Land Cover, (i) NDVI, (j) NDBI, (k) Distance to Rivers, (l) Distance to Roads, (m) Distance to Lineaments

4.3 Cone Penetration Test Results

CPT records from the four tested stations were interpreted using the soil behaviour type classification of Robertson et al. (1986). Three are presented here because they span the range of profiles encountered: a shallow clay profile over refusal (STA 7), a shallow profile with a coarser base (STA 10), and a thick, variable profile (STA 4).

At STA 7, refusal was reached at 1.4 m. Cone resistance rises steadily from 0.24 MPa at the surface to 2.26 MPa at refusal, and the friction ratio falls with depth, so the profile coarsens downward as overburden increases and water content decreases. Pore pressure stays low, between 0 and 3.5 kPa below 1 m. The soil behaviour type index falls from 3.46 to 2.39, indicating clay to 0.7 m, clay and silty clay between 0.7 and 1.1 m, and silty sand to sandy silt between 1.1 and 1.4 m.

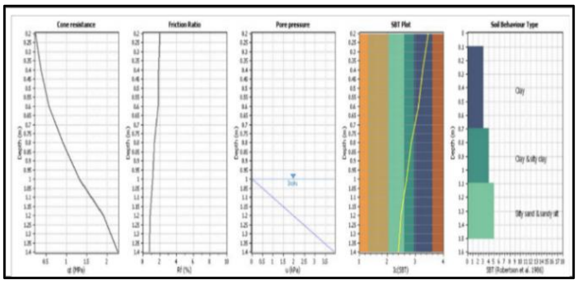

Figure 9. CPT Profile at STA 7

At STA 10, the profile extends to 1.8 m. Cone resistance increases from 0.59 to 2.45 MPa and pore pressure remains between 0 and 7 kPa, so the profile is not close to saturation at the time of testing. The friction ratio fluctuates, and the soil behaviour type index falls from 3.08 to 2.33: clay from 0.2 to 0.9 m, clay and silty clay to 1.3 m, and silty sand to sandy silt from 1.3 to 1.8 m.

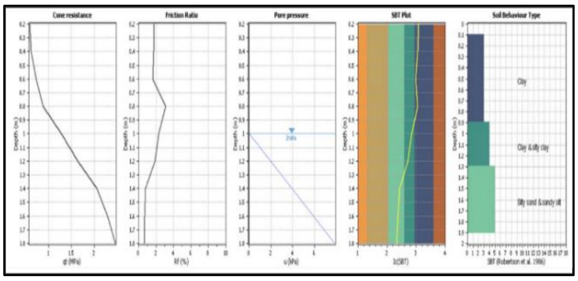

Figure 10. CPT Profile at STA 10

STA 4 gives the thickest record, 5.5 m. Cone resistance rises to about 1 m, falls between 1.2 and 2.6 m, then rises again to refusal, so the profile contains a weaker intermediate zone rather than a simple upward-coarsening sequence. Pore pressure is markedly higher here, up to about 45 kPa between 1 and 7 m, which is consistent with a perched water table in the clay. The soil behaviour type index ranges from 3.08 to 2.34 and gives clay from 0.2 to 0.5 m, clay and silty clay to 1.2 m, clay from 1.2 to 3.4 m, clay and silty clay to 4 m, and silty sand to sandy silt from 4 to 5.5 m.

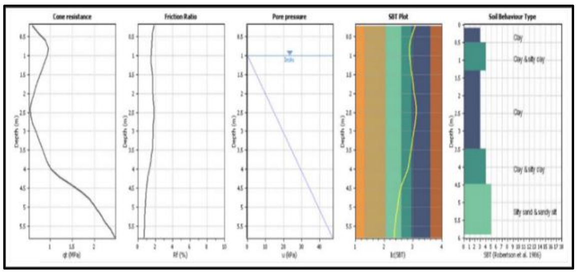

Figure 11. CPT Profile at STA 4

Two points matter for susceptibility. Every profile has a soft, low-resistance clay layer in the upper 1 to 1.5 m, which is the depth range in which the recorded shallow slides occur. And the higher pore pressures at STA 4 show that a perched water table can develop within the clay above the coarser base, which is the mechanism by which shear strength is lost during prolonged rainfall. STA 4 is also the station with the second steepest slope in the set and one of the six that return a factor of safety below 1.07, so the two conditions coincide there.

4.4. Soil Physical Properties

Physical property testing was carried out over approximately seven days. Results are given in Table 9.

Tabel 9. Results of Soil Physical Property Testing

Station	Water content w (%)	Specific gravity Gs	Unit weight γ (kN/m³)	Liquid limit LL (%)	Plastic limit PL (%)	Shrinkage limit SL (%)	Plasticity index PI (%)
STA 1	16.56	2.61	19.582	21.50	16.99	13.29	4.51
STA 2	21.21	2.58	19.213	39.00	23.76	16.51	15.24
STA 3	24.17	2.66	18.739	43.00	25.56	11.57	17.44
STA 4	23.79	2.57	19.847	31.25	23.41	11.07	7.84
STA 5	26.64	2.59	18.610	35.75	24.86	12.56	10.89
STA 6	25.02	2.63	19.068	33.50	21.46	14.37	12.04
STA 7	21.65	2.62	20.192	37.50	23.48	19.17	14.02
STA 8	37.95	2.46	18.490	54.00	30.14	22.13	23.86
STA 9	41.09	2.49	16.924	44.00	27.32	30.57	16.68
STA 10	18.57	2.56	19.815	25.75	18.54	22.01	7.21
STA 11	20.29	2.54	19.919	31.00	22.63	17.29	8.37
STA 12	24.74	2.57	15.760	58.50	31.82	11.20	26.68
STA 13	44.53	2.38	19.116	32.75	28.68	24.32	4.07
STA 14	23.25	2.65	18.988	47.50	27.06	9.48	20.44
STA 15	10.21	2.57	16.250	Non-plastic	Non-plastic	Non-plastic	0

Water content ranges from 10.21% to 44.53%, specific gravity from 2.38 to 2.66, and unit weight from 15.760 to 20.192 kN/m³. The narrow range of specific gravity is consistent with the geological setting described in Section 2.2: all four formations belong to the same basin fill, so the soils derive from mineralogically similar parent material. The wider spread of water content and unit weight reflects differences in saturation and density between stations rather than differences in mineralogy.

The Atterberg limits give LL between 21.50 and 58.50%, PL between 16.99 and 31.82%, and PI between 4.07 and 26.68%. Under Whitlow (1995), six stations fall in the low plasticity band, six in the medium band, and two, STA 8 and STA 12, in the high band. Applying Table 3, the soils classify as shown in Table 10.

Tabel 10. Plasticity Classification of the Tested Soils

Station	LL (%)	PI (%)	Liquid limit class	Soil type	Plasticity	Cohesion	Expansion potential from SL
STA 1	21.50	4.51	Low	Silt	Low	Slightly cohesive	Non-critical
STA 2	39.00	15.24	Medium	Silty clay	Moderate	Cohesive	Non-critical
STA 3	43.00	17.44	Medium	Clay	High	Cohesive	Moderate
STA 4	31.25	7.84	Low	Silty clay	Moderate	Cohesive	Moderate
STA 5	35.75	10.89	Medium	Silty clay	Moderate	Cohesive	Non-critical

Station	LL (%)	PI (%)	Liquid limit class	Soil type	Plasticity	Cohesion	Expansion potential from SL
STA 6	33.50	12.04	Low	Silty clay	Moderate	Cohesive	Non-critical
STA 7	37.50	14.02	Medium	Silty clay	Moderate	Cohesive	Non-critical
STA 8	54.00	23.86	High	Clay	High	Cohesive	Non-critical
STA 9	44.00	16.68	Medium	Silty clay	Moderate	Cohesive	Non-critical
STA 10	25.75	7.21	Low	Silty clay	Moderate	Cohesive	Non-critical
STA 11	31.00	8.37	Low	Silty clay	Moderate	Cohesive	Non-critical
STA 12	58.50	26.68	High	Clay	High	Cohesive	Moderate
STA 13	32.75	4.07	Low	Silt	Low	Slightly cohesive	Non-critical
STA 14	47.50	20.44	Medium	Clay	High	Cohesive	Critical
STA 15	Non-plastic	0	Non-plastic	Sand	Non-plastic	Non-cohesive	Non-plastic

Four stations are clay of high plasticity, eight are silty clay of moderate plasticity, two are silt of low plasticity, and one is non-plastic sand. Twelve of the fifteen stations are therefore cohesive fine-grained soils of moderate to high plasticity, which is the material that dominates the hilly part of the district.

Two relationships in these data are worth noting. LL and PI are almost perfectly correlated ($r = 0.959$, $p < 0.001$, $n = 14$), which is expected for a suite of soils with a comparable plastic limit and confirms internal consistency of the testing. Water content, in contrast, is only weakly related to LL ($r = 0.368$, $p = 0.195$) and to PI ($r = 0.327$, $p = 0.234$), neither of which is significant at $n = 15$. The natural water content at the time of sampling therefore reflects antecedent rainfall and drainage conditions at each site rather than the intrinsic plasticity of the soil, and it should not be read as an index of susceptibility on its own. STA 13 illustrates the point: it records the highest water content in the set, 44.53%, but the second lowest plasticity index, 4.07%.

STA 14 has a shrinkage limit of 9.48% and is critical for expansion, and STA 3, 4, and 12 are in the moderate band. On slopes these values matter because repeated shrink-swell during the dry-to-wet transition opens desiccation cracks that carry rainwater to depth and short-circuit the normal infiltration path.

4.5. Direct Shear Test and Slope Stability

Cohesion and internal friction angle from the direct shear test, the surveyed slope angle, and the factor of safety computed by the Morgenstern-Price method are given in Table 11.

Table 11. Direct Shear Test Results, Slope Geometry, and Factor of Safety

Station	Cohesion c (kPa)	Internal friction angle φ (°)	Slope angle β (°)	tan φ / tan β	Factor of safety	Interpretation
STA 1	0.0156	40.02	29	1.515	1.633	Safe
STA 2	0.5599	43.01	33	1.436	2.411	Safe
STA 3	0.5677	32.52	27	1.251	2.141	Safe
STA 4	0.2799	38.96	55	0.566	0.780	Unstable
STA 5	0.5988	13.97	59	0.149	0.515	Unstable
STA 6	0.3888	42.05	39	1.114	1.522	Safe
STA 7	0.2644	33.15	25	1.401	1.972	Safe

Station	Cohesion c (kPa)	Internal friction angle φ (°)	Slope angle β (°)	tan φ / tan β	Factor of safety	Interpretation
STA 8	0.1711	40.02	37	1.114	1.471	Safe
STA 9	0.2411	22.01	31	0.673	1.051	Unstable
STA 10	0.0106	57.93	34	2.366	2.424	Safe
STA 11	0.4510	7.96	26	0.287	0.961	Unstable
STA 12	0.0156	48.23	45	1.120	0.189	Unstable
STA 13	0.4355	24.27	36	0.621	1.435	Safe
STA 14	0.0078	60.78	40	2.131	2.187	Safe
STA 15	0.0156	26.45	47	0.464	0.514	Unstable

Cohesion is low throughout, between 0.0078 and 0.5988 kPa with a mean of 0.268 kPa, while the internal friction angle is comparatively high, ranging from 7.96° to 60.78° with a mean of 35.4°. Shear resistance in these soils is therefore supplied almost entirely by interparticle friction and mechanical interlocking rather than by cohesive bonding. That distinction has a direct consequence: frictional resistance depends on effective normal stress, so it degrades as pore water pressure rises during rainfall, whereas a genuinely cohesive soil would retain part of its strength.

The correlations across the fifteen stations make the controlling mechanism explicit. Cohesion has no detectable relationship with the factor of safety ($r = 0.071$, $p = 0.803$), and neither does the plasticity index ($r = 0.068$, $p = 0.809$). The internal friction angle on its own is only marginally related ($r = 0.498$, $p = 0.059$), and the slope angle on its own is significantly and negatively related ($r = -0.648$, $p = 0.009$). Neither variable explains the result alone, because a steep slope in strong material and a gentle slope in weak material can return the same factor of safety. Combining them does explain it: the ratio tan φ / tan β, which is the infinite-slope expression of frictional resistance against driving stress, correlates with the factor of safety at $r = 0.773$ ($p = 0.001$), and at $r = 0.886$ ($p < 0.001$) when the outlier discussed below is excluded. Cohesion and friction angle are themselves inversely related ($r = -0.570$, $p = 0.027$), the usual pattern for a suite of soils grading from clay to sand.

Six of the fifteen stations return a factor of safety below 1.07 and are classified as unstable: STA 4, 5, 9, 11, 12, and 15. The remaining nine exceed 1.25 and are classified as safe, and no station falls in the critical band. The unstable stations have a mean slope of 45.5° against 33.3° for the stable stations, and the difference is significant ($t = -2.77$, $p = 0.016$). The separation is close to categorical. Every one of the five stations on ground steeper than 40° is unstable, and of the ten stations at or below 40° only STA 11 is unstable, where the friction angle collapses to 7.96°. Material type does not separate the groups at all: the mean factor of safety by soil class is 1.50 for clay, 1.45 for silty clay, and 1.53 for silt, differences well within scatter.

STA 12 does not follow the pattern and should be treated with caution. Its friction angle of 48.23° on a 45° slope of bedded sandstone gives tan φ / tan β = 1.120, which is comparable to STA 6 and STA 8, yet the reported factor of safety is 0.189, the lowest in the set. The bedding at this station dips at 50°, steeper than the face itself, so a structurally controlled failure is plausible and would not be captured by a soil strength model. Either an additional condition applies at that site, such as a groundwater level or a weak layer in the model geometry that is not represented in the point strength data, or the analysis input needs rechecking. As explained in Section 3.3, the overall proportion of unstable stations is a property of the purposive sampling design and is not an estimate for the district.

4.6 Comparison between Stations

Table 12 brings the movement type, material classification, shear strength, slope geometry, and stability result together so that the stations can be compared directly.

Table 12. Comparative Summary of the Fifteen Observation Stations

Station	Movement type	Soil type (PI, %)	c (kPa)	φ (°)	β (°)	FS	Stability class
STA 1	Debris slide	Silt (4.51)	0.0156	40.02	29	1.515	1.633
STA 2	Debris slide	Silty clay (15.24)	0.5599	43.01	33	1.436	2.411
STA 3	Debris slide	Clay (17.44)	0.5677	32.52	27	1.251	2.141
STA 4	Rock and debris fall	Silty clay (7.84)	0.2799	38.96	55	0.566	0.780
STA 5	Successive rotational slide	Silty clay (10.89)	0.5988	13.97	59	0.149	0.515
STA 6	Debris slide	Silty clay (12.04)	0.3888	42.05	39	1.114	1.522
STA 7	Successive rotational slide	Silty clay (14.02)	0.2644	33.15	25	1.401	1.972
STA 8	Debris slide	Clay (23.86)	0.1711	40.02	37	1.114	1.471
STA 9	Debris slide	Silty clay (16.68)	0.2411	22.01	41	0.465	1.051
STA 10	Debris slide	Silty clay (7.21)	0.0106	57.93	34	2.366	2.424
STA 11	Earth slide	Silty clay (8.37)	0.4510	7.96	26	0.287	0.961
STA 12	Rock and debris fall	Clay (26.68)	0.0156	48.23	45	1.120	0.189
STA 13	Debris slide	Silt (4.07)	0.4355	24.27	36	0.621	1.435
STA 14	Successive rotational slide	Clay (20.44)	0.0078	60.78	40	2.131	2.187
STA 15	Successive rotational slide	Sand (NP)	0.0156	26.45	47	0.464	0.514

Three groups emerge when the stations are ordered by tan φ / tan β. The first is the low-resistance group, STA 5, 11, 15, 9, and 4, with ratios between 0.15 and 0.57 and a factor of safety between 0.51 and 1.05, all classified as unstable. Two mechanisms produce this: at STA 5 and STA 11 the friction angle collapses to 13.97° and 7.96°, while at STA 15, STA 9, and STA 4 the friction angle is moderate but the slope reaches 47°, 41°, and 55°. The second group contains STA 13 alone, with a ratio of 0.621 and a factor of safety of 1.435, which sits between the two extremes. The third group, STA 1, 2, 3, 6, 7, 8, 10, and 14, has ratios above 1.1 and a factor of safety between 1.47 and 2.42, and includes the two stations with the highest friction angles in the set, STA 10 and STA 14 at 57.93° and 60.78°. STA 12 falls outside the sequence for the reason given in Section 4.5.

Two results follow that bear directly on the spatial model. Slope angle and material properties are statistically independent across the fifteen stations (slope angle against friction angle, $r = -0.059$, $p = 0.833$), so the two carry separate information. And the material classification alone does not discriminate stability, since clay, silty clay, and silt return almost identical mean factors of safety, and the bedrock listed in Table 8 does not either, since sandstone underlies both the most and the least stable stations. Gradient is what varies systematically with stability, which is consistent with the outcome of the AUC screening reported in Section 4.7.

Comparing the stability class at each station with the susceptibility class assigned by the map at the same location provides the physical check described in Section 3.7. Agreement at a station means that the statistical model and the limit equilibrium analysis, which share no input data, reach the same conclusion at that point.

4.7 Weight of Evidence Results

Every class of every conditioning factor was assigned a positive weight, a negative weight, and a contrast using Equations 3 to 7, and the standard deviation of each weight and of the contrast was computed with Equation 8. Table 13 gives the results for the three factors retained in the final model, based on the 28 inventory points used in the weighting.

Table 13. Weights of Evidence for the Classes of the Five Dominant Conditioning Factors

Factor	Class	Points	W^+	$s(W^+)$	W^-	$s(W^-)$	C	s(C)
Slope angle	1	0	−1.6525	1.4907	0.0769	0.2389	−1.7294	1.5097
Slope angle	2	1	−2.2370	0.8393	0.7019	0.2809	−3.0289	0.8851
Slope angle	3	2	−1.2798	0.6816	0.2809	0.2583	−1.5607	0.7289
Slope angle	4	13	2.2311	0.6885	−0.5752	0.2925	2.8063	0.7481
Slope angle	5	12	2.2514	0.6928	−0.5126	0.2858	2.6668	0.7494
Slope aspect	1	0	−1.6525	1.4907	0.0769	0.2389	−1.7294	1.5097
Slope aspect	2	1	−2.3270	0.8393	0.7019	0.2809	−3.0289	0.8851
Slope aspect	3	2	−1.2798	0.6816	0.2809	0.2583	−1.5607	0.7289
Slope aspect	4	13	2.2311	0.6885	−0.5752	0.2925	2.8063	0.7481
Slope aspect	5	12	2.1542	0.6928	−0.5126	0.2858	2.6668	0.7481
Elevation	1	1	1.6433	1.6330	−0.0431	0.2378	1.6864	1.6502
Elevation	2	1	−2.4342	0.8370	0.8385	0.2918	−3.2727	0.8864
Elevation	3	26	0.8014	0.2941	−1.9234	0.6587	2.7248	0.7214

The pattern is consistent across the three factors. For slope angle, classes 4 and 5 contain 25 of the 28 inventory points and carry large positive contrasts, 2.8063 and 2.6668, while the three gentler classes carry negative contrasts down to −3.0289. Susceptibility therefore rises with gradient, and the transition is sharp rather than gradual: the contrast changes sign between class 3 and class 4. Slope aspect behaves the same way, with the two classes that face the dominant rain-bearing direction accounting for the same 25 points and returning contrasts of 2.8063 and 2.6668, which is consistent with longer wetting and slower drying on those faces. For elevation, class 3 alone contains 26 of the 28 points and returns a contrast of 2.7248, separating the dissected hills from the alluvial plain.

The standard deviation of the contrast measures how firmly each association is established. It is small for the classes that carry most of the inventory, 0.7481 and 0.7494 for slope angle classes 4 and 5 and 0.7214 for elevation class 3, so those associations are well constrained. It is large for the classes with no or almost no points, 1.5097 for slope class 1 and 1.6502 for elevation class 1, which is expected because a weight computed from a single point carries little information. The negative contrast of the gentle and low classes should therefore be read as an absence of recorded failures rather than as demonstrated stability.

These results agree with the field measurements reported in Section 4.5. The stations that returned a factor of safety below 1.07 average 45.5° in slope against 33.3° for the stable ones, and every station steeper than 40° was unstable, which is the same threshold behaviour that appears between slope classes 3 and 4 in Table 13.

Each of the thirteen factors was then screened by its individual AUC (Table 14).

Table 14. Individual AUC of Each Conditioning Factor

Rank	Conditioning factor	AUC	Retained
1	Slope angle	0.8980	Yes
2	Slope aspect	0.8980	Yes
3	Elevation	0.7475	Yes

Rank	Conditioning factor	AUC	Retained
4	Soil type	0.6893	No
5	Distance to rivers	0.6069	No
6	Land cover	0.6062	No
7	Distance to lineaments	0.5305	No
8	Profile curvature	0.5221	No
9	Plan curvature	0.5057	No
10	Distance to roads	0.4814	No
11	NDVI	0.4039	No

Three factors exceed the 0.7 threshold and were carried into the overlay: slope angle, slope aspect, and elevation. All three are terrain derivatives, which means the spatial model discriminates on geometry alone.

Two exclusions deserve comment because they are informative rather than merely negative. Soil type reaches only 0.6893 and does not enter the model. On its own that could be read as a failure of the soil layer, but the station data explain it: the mean factor of safety is 1.50 for clay, 1.45 for silty clay, and 1.53 for silt, and the plasticity index shows no relationship with the factor of safety ($r = 0.068$, $p = 0.809$). The material across the hilly part of the district is uniformly weak and uniformly frictional, so the soil map cannot separate ground that failed from ground that did not. This is a case where the geotechnical measurements confirm a statistical result that would otherwise look like a data problem. Distance to roads (0.4814) and NDVI (0.4039) fall below 0.5, which means they are inversely associated with the inventory at this extent and carry no usable signal.

The model therefore predicts where the driving stress is highest, while the geotechnical results in Sections 4.4 and 4.5 supply the reason the material yields once that stress is applied. Neither part is sufficient alone, which is the argument for combining them.

4.8 Model Validation

The ROC curve for the final model rises steeply from the origin, so the highest susceptibility values already capture a large share of the inventory, then flattens once specificity reaches about 0.4, at which point all recorded events have been detected. The curve stays above the diagonal reference line throughout and does not fall back. The model returns an AUC of 0.863 (Figure 12), which is a good level of predictive performance under Table 6, and means that a randomly chosen mass movement location has an 86.3% probability of being assigned a higher susceptibility index than a randomly chosen stable location.

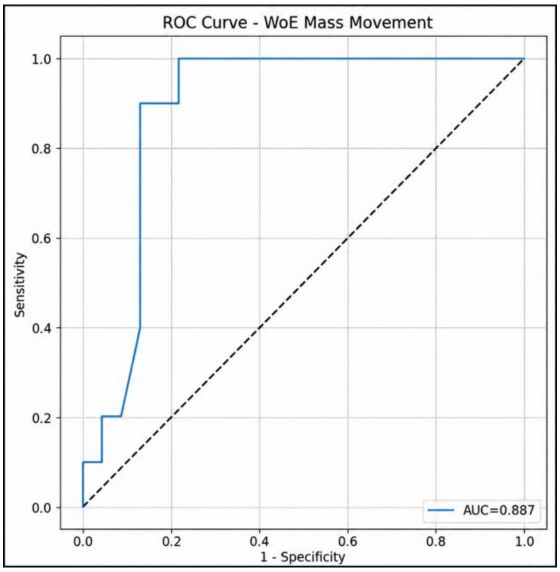

Figure 12. ROC curve for the Weight of Evidence model

Submitted January 2026, Revised August 2026, Accepted August 2026, Published August 2026

Validation is also supported from a second, independent direction. The station-scale limit equilibrium results in Table 12 share no input data with the WoE model, since the model uses terrain derivatives while the factor of safety uses measured c, φ, unit weight, and surveyed slope geometry. Agreement between the two at the station locations is therefore a stronger test than a statistical curve computed from the same inventory that trained the weights.

4.9 Mass Movement Susceptibility Map

The susceptibility index was normalised and reclassified into three levels using the BNPB (2019) thresholds. The result is shown in Figure 13 and the class areas in Table 15.

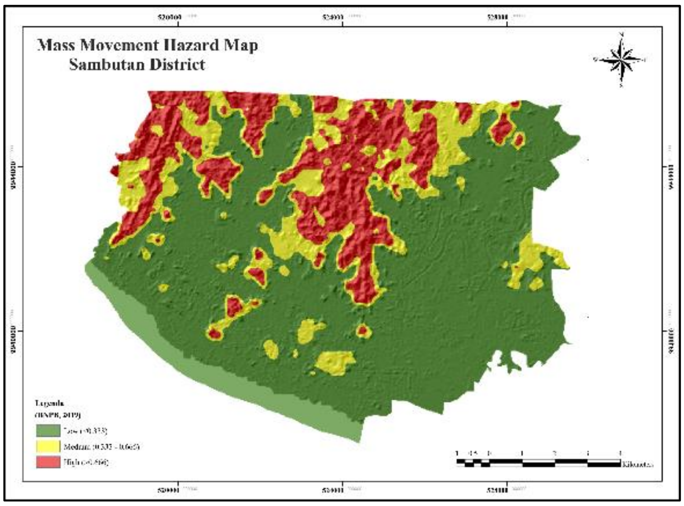

Figure 13. Mass Movement Susceptibility Map of Sambutan District

Table 15. Distribution of Susceptibility Classes

Susceptibility class	Index range	Area (km²)	Proportion (%)
Low	< 0.333	62.05	54.72
Moderate	0.333–0.666	9.98	8.80
High	> 0.666	41.37	36.48
Total		113.40	100.00

The low class covers 62.05 km², slightly over half the district, and occupies the gentle terrain of the alluvial plain and the lower footslopes. The moderate class is the smallest at 9.98 km² and forms a narrow north-south belt with extensions to the west and northwest and a few isolated patches in the east; these are transitional slopes where a change in gradient or a new cut would move the ground into the high class. The high class covers 41.37 km², more than a third of the district, and runs from the north to the south of the area with additional concentrations in the northwest and southwest.

The geotechnical results explain why the high class occupies the ground it does. Twelve of the fifteen stations are clay or silty clay of moderate to high plasticity, which absorbs and holds water and reaches saturation quickly under sustained rainfall. Cohesion in this material is negligible, below 0.6 kPa at every station, so resistance comes almost entirely from friction, and friction depends on effective normal stress. As saturation increases, pore water pressure rises, effective stress falls, and the only significant component of resistance is lost. Whether that loss produces failure depends on how much margin the slope had to begin with, which is why the ratio tan φ / tan β predicts the factor of safety ($r = 0.773$) while material class and cohesion do not. This is also why the spatial model retains only terrain derivatives: the weak frictional material is present almost everywhere in the hilly part of the district, so it cannot discriminate failed from unfailed ground, and what varies from place to place is the gradient acting on it. The high class therefore marks where that gradient is steep enough to exhaust the margin.

The CPT profiles add the geometry of the problem: a soft clay layer 1 to 1.5 m thick over a firmer, coarser base occurs at all four stations tested, which is the classic configuration for shallow translational sliding and matches the debris slides that dominate the inventory. The elevated pore pressure recorded at STA 4 confirms that a perched water table can develop at that contact, and STA 4 is one of the six stations with a factor of safety below 1.07.

The narrowness of the moderate class, only 8.8% of the area, is itself informative. The transition from stable to unstable ground in this district is abrupt rather than gradual, because it follows the break in slope between the alluvial plain and the dissected hills rather than a slow change in material. The station data support this reading, since the material classification is almost uniform across the stations while the slope angle is not, and the contrast values in Table 13 change sign abruptly between slope classes 3 and 4. For planning purposes the boundary of the high class should be treated as a real line on the ground and not as the centre of a broad transition zone.

4.10 Implications for Spatial Planning and Mitigation

Susceptibility maps are used by planners, not by geotechnical engineers, so the results above are translated here into measures that can be written into the RTRW and RDTR of Samarinda City. Because the station data show that gradient rather than material is what separates stable from unstable ground, the measures below are organised around controlling slope geometry and keeping the soil unsaturated.

For land use allocation, the high susceptibility class should be directed towards protected function, green open space, and low-density agroforestry rather than towards residential expansion. Where residential use already exists inside the class, the RDTR should cap building coverage and prohibit further subdivision, since added impervious surface concentrates runoff onto the slope. New residential and infrastructure growth should be directed to the low class, which occupies 62.05 km² and is more than sufficient for the projected demand of the district.

For slope geometry, which is the strongest control identified in this study, the RDTR should set a gradient threshold. Every station on ground steeper than 40° returned a factor of safety below 1.07, and the six unstable stations average 45.5° against 33.3° for the stable ones. Development on natural slopes steeper than 40° should therefore be prohibited without engineered stabilisation, and any cut that would create a face steeper than the natural gradient should require analysis demonstrating a factor of safety of at least 1.5 for permanent slopes under static conditions, in accordance with SNI 8460:2017. Cuts should be benched rather than continuous, and fill placement on slope crests should be prohibited, because added crest load raises the driving moment on precisely the slip surface geometry that the CPT profiles indicate.

For building permits, the RDTR should require a site-specific geotechnical investigation before any permit is issued inside the high class, comprising at least one CPT or borehole per building footprint taken to refusal or to firm ground, together with laboratory determination of the Atterberg limits and the shear strength parameters. This requirement follows from the measurements reported here: the internal friction angle varies from 7.96° to 60.78° between stations barely a kilometre apart, and neither the soil map unit nor the plasticity index predicts it, so no district-wide design assumption is defensible and the properties must be measured at the site. Buildings within the high class should be restricted to low-rise, light structures unless the slope is stabilised and the foundations are carried through the soft mantle into the firmer layer identified by CPT.

For drainage, water management is the single most effective measure available, because the failure mechanism identified in Sections 4.3 to 4.5 is the loss of frictional resistance when pore pressure rises in a soil that has almost no cohesion to fall back on. Lined interceptor drains should be installed along slope crests to divert runoff before it reaches the face; drainage channels should be lined rather than earthen, since unlined channels on plastic clay leak into the very layer that must stay unsaturated; and horizontal or counterfort subsurface drains should be installed at sites where a perched water table forms above the coarser base, of which STA 4 is the clearest example. Channels should be cleared before the onset of the wet season. At the four stations with moderate to critical expansion potential, in particular STA 14, surface protection to limit desiccation cracking should be added, because open cracks admit rainwater directly to the potential slip surface.

For monitoring and preparedness, the settlements inside the high class should be covered by a rainfall-threshold early warning arrangement operated with BPBD, and the recording of events should continue and be geolocated, since a larger inventory would allow the model to be rebuilt for individual movement types rather than for mass movement as a whole.

5. Conclusion

This study set out to characterise the slope-forming materials of Sambutan District, to identify the factors most strongly associated with recorded mass movement, to produce and validate a susceptibility map, and to translate the result into spatial planning terms.

Twelve of the fifteen stations are clay or silty clay of moderate to high plasticity, with a plasticity index between 4.07 and 26.68%, cohesion between 0.0078 and 0.5988 kPa, and internal friction angles between 7.96° and 60.78° on slopes of 25° to 59°. Shear resistance is supplied almost entirely by friction rather than cohesion. Neither cohesion ($r = 0.071$, $p = 0.803$), plasticity index ($r = 0.068$, $p = 0.809$), nor friction angle alone ($r = 0.498$, $p = 0.059$) predicts the factor of safety, but the ratio $\tan \varphi / \tan \beta$ does ($r = 0.773$, $p = 0.001$), which identifies the interaction of material strength with slope geometry as the controlling mechanism. Six of the fifteen stations return a factor of safety below 1.07, and these average 45.5° in slope against 33.3° for the remaining nine ($p = 0.016$). Every station on ground steeper than 40° is unstable. The CPT profiles show a soft clay layer 1 to 1.5 m thick over a firmer base at all four stations tested, and elevated pore pressure at STA 4 confirms that a perched water table can form at that contact.

Of the conditioning factors tested, three exceed an individual AUC of 0.7 and were retained: slope angle (0.898), slope aspect (0.898), and elevation (0.7475). Soil type reaches only 0.6893 and was excluded, which the station data explain rather than contradict, since the mean factor of safety is almost identical for clay, silty clay, and silt. The weights confirm the threshold behaviour seen in the field: the two steepest slope classes contain 25 of the 28 inventory points and carry contrasts of 2.8063 and 2.6668, while the gentler classes carry negative contrasts.

The Weight of Evidence model reached an AUC of 0.863, which is a good level of predictive performance under the criteria of Yesilnacar and Topal (2005). The resulting map assigns 62.05 km² (54.72%) of the district to the low class, 9.98 km² (8.80%) to the moderate class, and 41.37 km² (36.48%) to the high class.

The advantage of the approach lies in the combination rather than in either component. Weight of Evidence derives its weights from the observed association between the inventory and each factor class, so the model is reproducible and free of the expert scoring that scoring-based methods require, and its positive weight, negative weight, and contrast are directly interpretable class by class. Adding measured geotechnical parameters supplies what a purely spatial model cannot: a physical explanation of why the high class fails, and an independent check on the zonation at fifteen points, since the limit equilibrium analysis and the statistical model share no input data. In this case the geotechnical data also explain a result that a spatial model alone would have left unresolved. The soil type layer failed the AUC screening, which in isolation would look like a defect in the input data; the station measurements show instead that the material is uniformly weak across the hilly part of the district and that gradient is what varies, so the exclusion is a real property of the setting rather than an artefact. This is the element missing from the comparable studies listed in Table 1.

For policy, the results support four measures inside the high susceptibility class: allocation to protected function and green open space in the RDTR; a gradient threshold prohibiting development on natural slopes steeper than 40° without engineered stabilisation, with cut slopes designed to a factor of safety of at least 1.5 under SNI 8460:2017 and fill on slope crests prohibited; a mandatory site-specific geotechnical investigation before any building permit, since the friction angle varies from 7.96° to 60.78° over distances of about a kilometre; and lined crest drainage with subsurface drainage where a perched water table is present. New residential growth should be directed to the low class, which has ample capacity for the projected demand of the district.

The main limitations are the size of the inventory, 33 events, which is sufficient for a general susceptibility model but not for separate models by movement type; the purposive sampling of the fifteen stations, which deliberately targets failure-prone ground; the single anomalous stability result at STA 12, which does not follow the relationship established by the other fourteen stations; the fact that the retained factors are all terrain derivatives, so the map predicts driving stress well but represents material behaviour only through the accompanying geotechnical data; and the absence of a temporal component, since a susceptibility map states where failure is likely and not when. Future work should extend the inventory, add rainfall-threshold analysis to convert susceptibility into time-dependent hazard, and test whether a geotechnically informed soil layer improves other models such as logistic regression or random forest.

Acknowledgments

The authors thank all parties who contributed to this research, in particular the Badan Penanggulangan Bencana Daerah of Samarinda City for access to the mass movement inventory, and the Civil Engineering Laboratory of the Faculty of Engineering, Universitas Mulawarman, for the use of laboratory facilities.

References

Akbar, T. A., Hassan, Q. K., Ishaq, S., Batool, M., Butt, H. J., & Jabbar, H. (2019). Investigative spatial distribution and modelling of existing and future urban land changes and its impact on urbanization and economy. *Remote Sensing*, *11*(2). https://doi.org/10.3390/rs11020105

Allan Takwin, G., E. T. A., & Rondonuwu, S. G. (2017). *Analisis Kestabilan Lereng Metode Morgenstern-Price (Studi Kasus : Diamond Hill Citraland)*. *15*(67).

Altmeyer, W. T. (1955). Discussion of engineering properties of expansive clays. *Transactions of the American Society of Civil Engineers, 121*(1), 666–669.

Badan Nasional Penanggulangan Bencana. (2019). *Kajian risiko bencana Indonesia*. Jakarta: BNPB.

Badan Penanggulangan Bencana Daerah Kota Samarinda. (2023). *Data kejadian bencana Kota Samarinda*. Samarinda: BPBD Kota Samarinda.

Badan Standardisasi Nasional. (2008a). *SNI 1964:2008 Cara uji berat jenis tanah*. Jakarta: BSN.

Badan Standardisasi Nasional. (2008b). *SNI 1965:2008 Cara uji penentuan kadar air untuk tanah dan batuan di laboratorium*. Jakarta: BSN.

Badan Standardisasi Nasional. (2008c). *SNI 1966:2008 Cara uji penentuan batas plastis dan indeks plastisitas tanah*. Jakarta: BSN.

Badan Standardisasi Nasional. (2008d). *SNI 1967:2008 Cara uji penentuan batas cair tanah*. Jakarta: BSN.

Badan Standardisasi Nasional. (2008e). *SNI 2813:2008 Cara uji kuat geser langsung tanah terkonsolidasi dan terdrainase*. Jakarta: BSN.

Badan Standardisasi Nasional. (2008f). *SNI 3422:2008 Cara uji analisis ukuran butir tanah dan batas susut*. Jakarta: BSN.

Badan Standardisasi Nasional. (2017). *SNI 8460:2017 Persyaratan perancangan geoteknik*. Jakarta: BSN.

Bonham-Carter, G. F. (1994). *Geographic information systems for geoscientists: Modelling with GIS*. Oxford: Pergamon.

Bowles, J. E. (1989). *Physical and geotechnical properties of soils* (2nd ed.). New York: McGraw-Hill.

Cruden, D. M., & Varnes, D. J. (1996). Landslide types and processes. In A. K. Turner & R. L. Schuster (Eds.), *Landslides: Investigation and mitigation* (Special Report 247, pp. 36–75). Washington, DC: Transportation Research Board, National Research Council.

Das, B. M. (2010). *Principles of geotechnical engineering* (7th ed.). Stamford: Cengage Learning.

Gofar, N., & Ismail, M. (2022). Pemetaan Sebaran Jenis dan Kondisi Tanah berdasarkan data Sondir (CPT) menggunakan Sistem Informasi Geografis Mapping of Soil's Type and Condition based on CPT Using Geographical Information System. In *Jurnal Manajemen Aset Infrastruktur & Fasilitas* (Vol. 6, Issue 1). http://bappedalitbang.palembang.go.id.

Hardiyatmo, H. C. (1995). *Mekanika tanah I*. Jakarta: PT Gramedia Pustaka Utama.

Karunarathna, S., Bandara, P., Goto, S., & Bandaranayake, S. (2024). Identification of potential natural slope failure zones by geomorphological analyses using raster slope shading of LiDAR: Case study from Kegalle, Sri Lanka. In *Progress in landslide research and technology* (Vol. Part F4148, pp. 363–377). Springer Nature. https://doi.org/10.1007/978-3-031-55120-8_26

Kusmajaya, S., Tjahjono, B., & Barus, B. (2022). Bahaya longsor di Kabupaten Sukabumi berbasis metode Weight of Evidence (WoE), Logistic Regression (LR) dan kombinasi WoE-LR. *Jurnal Ilmu Tanah dan Lingkungan, 22*(2), 101–106. https://doi.org/10.29244/jitl.22.2.101-106

Liao, M., Wen, H., & Yang, L. (2022). Identifying the essential conditioning factors of landslide susceptibility models under different grid resolutions using hybrid machine learning: A case of Wushan and Wuxi counties, China. *Catena, 217*, 106428.

Ling, X., Zhu, Y., Ming, D., Chen, Y., Zhang, L., & Du, T. (2022). Feature engineering of geohazard susceptibility analysis based on the random forest algorithm: Taking Tianshui City, Gansu Province, as an example. *Remote Sensing, 14*(22), 5658. https://doi.org/10.3390/rs14225658

Lunne, T., Powell, J. J. M., & Robertson, P. K. (2014). *Cone penetration testing in geotechnical practice*. Boca Raton: CRC Press.

Morgenstern, N. R., & Price, V. E. (1965). The analysis of the stability of general slip surfaces. *Géotechnique, 15*(1), 79–93.

Murthy, V. N. S. (2006). *Geotechnical engineering*. New York: Marcel Dekker.

Niu, Q., Dang, X., Li, Y., Zhang, Y., Lu, X., & Gao, W. (2018). Suitability analysis for topographic factors in loess landslide research: A case study of Gangu County, China. *Environmental Earth Sciences, 77*, 294.

Pourghasemi, H. R., Pradhan, B., Gokceoglu, C., Mohammadi, M., & Moradi, H. R. (2013). Application of weights-of-evidence and certainty factor models and their comparison in landslide susceptibility mapping. *Arabian Journal of Geosciences, 6*(7), 2351–2365.

Priyono. (2015). Hubungan klasifikasi longsor, klasifikasi tanah rawan longsor dan klasifikasi tanah pertanian rawan longsor. *Gema*.

Regmi, N. R., Giardino, J. R., & Vitek, J. D. (2010). Modeling susceptibility to landslides using the weight of evidence approach: Western Colorado, USA. *Geomorphology, 115*(1–2), 172–187.

Robertson, P. K. (1990). Soil classification using the cone penetration test. *Canadian Geotechnical Journal, 27*(1), 151–158.

Robertson, P. K., Campanella, R. G., Gillespie, D., & Greig, J. (1986). Use of piezometer cone data. In *Use of in situ tests in geotechnical engineering* (Geotechnical Special Publication No. 6, pp. 1263–1280). New York: ASCE.

Saha, A., Mandal, S., & Saha, S. (2020). Geo-spatial approach-based landslide susceptibility mapping using analytical hierarchical process, frequency ratio, logistic regression and their ensemble methods. *SN Applied Sciences, 2*(10). https://doi.org/10.1007/s42452-020-03441-3

Supriatna, S., Sukardi, & Rustandi, E. (1995). *Peta geologi lembar Samarinda, Kalimantan Timur*. Bandung: Pusat Penelitian dan Pengembangan Geologi.

Tania, E., & Wulandari, T. E. (2020). Analisis korelasi kuat geser tanah menggunakan uji triaksial dan uji direct shear test Nickel Smelter Kalimantan Timur. *Journal of Applied Science Engineering*, 21–29.

van Westen, C. J., Rengers, N., & Soeters, R. (2003). Use of geomorphological information in indirect landslide susceptibility assessment. *Natural Hazards, 30*(3), 399–419.

Whitlow, R. (1995). *Basic soil mechanics*. Malaysia: Longman.

Wubalem, A., & Meten, M. (2020). Landslide susceptibility mapping using information value and logistic regression models in Goncha Siso Eneses area, northwestern Ethiopia. *SN Applied Sciences, 2*(5). https://doi.org/10.1007/s42452-020-2563-0

Yesilnacar, E., & Topal, T. (2005). Landslide susceptibility mapping: A comparison of logistic regression and neural networks methods in a medium scale study, Hendek region (Turkey). *Engineering Geology, 79*(3–4), 251–266.

Zakaria, Z., Sophian, I., Sabila, Z. S., & Jihadi, L. H. (2018). Slope safety factor and its relationship with angle of slope gradient to support landslide mitigation at Jatinangor education area, Sumedang, West Java, Indonesia. *IOP Conference Series: Earth and Environmental Science, 145*(1), 012052. https://doi.org/10.1088/1755-1315/145/1/012052

Zuidam, R. A. (1985). Aerial Photo-Interpretation in Terrain Analysis and Geomorphology Mapping. *Smits Pulb, Enchede. ITC*, The Netherlands